JMEPEG (2007) 16:559–566
DOI: 10.1007/s11665-007-9083-6

1059-9495/$19.00

Mechanical Properties of Reinforcing Steel and Fatigue Behavior in Corrosive Environment

Ch.Alk. Apostolopoulos and D. Michalopoulos

(Submitted June 15, 2006; in revised form August 23, 2006)

Corrosion of reinforcing steel has a great impact on the mass reduction and high- and low-cycle fatigue. An experimental study showed that the mass loss, the fatigue limit and the life expectancy were reduced by approximately 1.50-3.00%, 20-40%, and 55-75%, respectively, according to the level of corrosion. Low-cycle strain controlled fatigue testing under ±1% and ±2.5% constant amplitude strain, indicated that the corroded steel bars exhibit gradual reduction in available energy, number of cycles to failure and the load-bearing ability. Formation of pits and notches took place on the corroded steel surface and stress concentration points were developed which are highly localized at imperfections and especially at the rib bases. The fatigue limit was reduced considerably since the existence of ribs and the formation of pits and notches combined with the mass loss led to reduction of the exterior hard layer of martensite and drastic drop in the energy density of the corroded specimens. Antiseismic design that does not take into account the maximum and cumulative plastic deformation demands and the strain history that a structure will suffer under severe ground motion could lead to unpredictable performance.

Keywords $BSt500_s$ steel, corrosion, fatigue, low-cycle fatigue, mass loss

1. Introduction

Corrosion of reinforcing steel is a serious problem and observations on numerous structures show that corrosion of reinforcing steel is a prime factor contributing to the cracking and spalling of concrete. When structures are exposed to aggressive environments and when the concrete protection is deteriorated, corrosion of the reinforcement is initiated. Rust, the corrosion product of iron, is the result of an electrochemical process during which metallic iron is converted to iron oxide, creating volumetric expansion of the steel bars and also causing extremely high-tensile forces within the concrete cover. This results in crack formation from the steel bar to the concrete surface or between bars allowing oxygen and moisture to attack the bars faster and increase the corrosion rate. The rust reduces the bond strength and results in the loss of steel-concrete composite action, which affects the serviceability and performance of structures (Ref 1-5).

The corrosion products have much greater volume than the metal from which they form and this volume increase exerts great disruptive tensile stress on the surrounding concrete. When the pressure is such that the tensile stress in the concrete cover is greater than its own tensile strength, the concrete cracks leading to further corrosion. Corrosion cracks are usually parallel to the reinforcement, and are thus quite distinct from transverse cracks associated with tension in the reinforcement caused by loading. As the corrosion proceeds, the longitudinal cracks widen and, together with structural transverse cracks, may cause spalling of the concrete.

Rust occurs because of differences in electrical potential between small areas on the steel surface involving anodes, cathodes and an electrolyte. These differences in potential on the steel surface are caused by:

- Variations in composition structure
- Presence of impurities
- Uneven internal stress
- Presence of nonuniform environment.

While steel corrosion is the main cause affecting concrete durability, the relationship between corrosion level and load carrying capacity of structural members has not been established yet. Steel corrosion and associated cracking and spalling of concrete have been identified as the most severe forms of deterioration. At rebar corrosion of about 7 and 12% the rib profile loss is around 45 and 70% accordingly, which explains the steel bar slippage mode of failure. Corrosion levels of 5 and 7% are observed to cause significant increase in crack width and rib profile loss and 30-70% reduction in bond strength. A crack width of about 0.30 mm and 25% rib profile loss appear to be the threshold beyond which a sharp reduction in bond strength occurs (Ref 6, 7).

Corrosion is usually underestimated since the concrete provides physical protection to the steel by the dense and relatively impermeable structure of this material. The thin oxide layer covering the reinforcement, during concrete hydration, ensures chemical protection. The oxide layer remains stable in the alkaline concrete environment, pΘ 12.5-13.0, but begins to deteriorate when the pH of the pore solution drops below 11 (Ref 8, 9). The corrosion deterioration rate rises when the pH drops below nine. For corrosion to commence, the oxide film

Ch.Alk. Apostolopoulos and **D. Michalopoulos,** Department of Mechanical Engineering and Aeronautics, University of Patras, Patras 26500, Greece. Contact e-mail: mixalop@mech.upatras.gr.

must be broken or depassivated, which may occur if the alkalinity of the pore water in the concrete pores decreases and/or penetration of the chloride ions takes place. This may be caused by carbonation, especially in the proximity of cracks, or by water dilution, which accompanies cracking (Ref 4, 10). The advancing corrosion results to a reduction of the load carrying cross section of the bars and an increase of their volume by 3-8 times (Ref 11). The volume increase causes the build up of internal stresses, which cause cracking or even spalling of the concrete cover, which in turn further accelerates corrosion rates. Advancing corrosion leads to an appreciable decrease on the bond strength between the reinforcing bars and concrete (Ref 12, 13).

Seismic loads act on the load-bearing elements of structures in the form of high-strain reversals, which can be simulated as single axis low-cycle fatigue (Ref 14]. The Fourier spectra (Ref 15) of ground movement during an earthquake that occurred in Japan showed that the loading was cyclic and the frequency corresponding to the maximum amplitude was approximately 2 Hz. Investigation of the catastrophic earthquake of Tang Shan in China confirmed that the failure mode of the building structural steel was low-cycle fatigue (Ref 14). During seismic movement, structures are subjected to alternating shear forces and bending moments. This cyclic motion results in the gradual bursting and detachment of the concrete cover, which finally leaves the reinforcing steel bars as the sole load-bearing elements thus forcing them to carry both the shear forces and the bending moments, leading to permanent plastic deformation of the steel. These deformations increase due to the continuous dynamic loading while the compressive concrete zone is annihilated (Ref 16).

In coastal locations the climatic conditions constitute one of the most aggressive environments for concrete structures due to the severe ambient salinity, high temperature and humidity and also due to the ingress of chlorine through wind borne salt spray (Ref 7, 17). Chloride induced damage of reinforcing steel results in concrete cracking and spalling, destruction of the protective steel barrier and formation of pits, notches, and cavities on the steel surface. Durability is one of the most important merits of using reinforced concrete; however, formation of cracks causes corrosion of the steel bars and initiation of a serious problem, which becomes more severe in harsh environments. Even though the impact of corrosion on the strength of steel reinforcing bars is well known the current design codes do not face the problem since they are unable to quantify it and need further review. It has been attempted to quantify corrosion and mass loss of steel with the reduction of its mechanical properties (Ref 17, 18). The annual repair cost for highway bridges in the United States due to soluble chlorides, including steel and concrete, is estimated to $8.3 billion while the corresponding cost for highways is $20 billion (Ref 19, 20) and indirect costs due to traffic delays and lost productivity is estimated at more than 10 times the direct cost.

Reinforced concrete structures are seriously affected by steel corrosion due to exposure to chlorides from seawater, salt and saltwater, deicing chemicals, brackish water or spray from these sources. In addition steel-concrete bonding is greatly reduced through deterioration of the steel, concrete, or both (Ref 5, 21). Rust resides at the interface between steel reinforcement and concrete, degrading their bond and also reducing the useful life of the structure. The reduction in the structural performance of reinforced concrete members due to corroded steel is caused by the loss in the effective cross-sectional area of concrete due to cracking in the cover concrete, loss in the mechanical properties (Ref 17, 18) and performance of reinforcing bars due to reduction of their cross-sectional area and also loss of bonding (Ref 5, 21, 22).

Low-cycle fatigue of rebar occupies a large extent of the research results. It is felt that such amount of results still need time and work to be properly processed in order to arrive at a quantitative analytical model able to embrace all features only qualitatively described (Ref 23-26). The level of corrosion of steel bars affects their durability and performance and shortens the design life of structures (Ref 27-30). Designers of antiseismic structures are mostly concerned with issues of high- and low-cycle fatigue and their impact on the life expectancy of structures. Similar investigations but with noncorroded specimens were conducted by other researchers as well (Ref 31, 32).

In the present study the impact of corrosion on mass loss, high- and low-cycle fatigue properties of BSt500s steel, used extensively in Greece between 1990 and 2005, was evaluated because no similar study was found in the literature.

2. Experimental Procedure

2.1 Induced Corrosion

$BSt500_s$ steel in maximum permissible values of the final product contains C = 0.240%, P = 0.055%, S = 0.055% and N = 0.013% with the mechanical properties shown in Table 1.

Ribbed steel bars 12 mm in diameter were artificially corroded in a specially designed salt spray corrosion chamber, according to ASTM B117-94 standard, for 10, 20, 30, 45, 60, and 90 days. To accelerate corrosion the specimens were sprayed in a 5% sodium chloride and 95% distilled water solution, with pH range of 6.5-7.2 and spray chamber temperature of $35\pm^{1.1}_{1.7}$°C for different exposure times so that different corrosion levels were obtained. Pitting was observed to have started progressively on the specimens after 10, 20, and 30 days corrosion level which became progressively more severe. After salt spray exposure the specimens were washed with clean water according to ASTM G 1-72 procedure in order to remove any left over salt deposits from their surface and then dried.

2.2 Mass Loss

The steel corrosion level was measured as the fraction of the difference between the initial and final masses M_i and M_f, before and after completion of the corrosion process, divided by M_i, multiplied by 100.

The relationship between the remaining mass and corrosion duration for corroded vs. noncorroded specimens is shown in Fig. 1. The area A_s used in the calculation of the fatigue stress was determined according to DIN 488-3 specification as

$$A_s = \frac{1.274 \times M_f}{l} \quad \text{(Eq 1)}$$

where A_s is in mm^2, M_f is in g and l is the length in mm. The corrosion process created pitting and formed cavities and notches on the steel surface and especially the rib bases, which became more severe as the corrosion level increased, as shown in the stereoscopic images of Fig. 2. The relatively large pits at 30 days of salt spray exposure suggest that these are the active sites at which corrosion is primarily taking place. Pitting

appeared to be initiated at the reinforcement veins of the steel bars and proceeded to the intermediate space.

The gradual decrease of the strength characteristics is related to the mass loss and in particular of the more resistive martensitic outer layer. The micrographs of Fig. 3 show the gradual decrease of the thickness of the martensitic outer shell with increasing corrosion level.

Table 1 Mechanical properties of steel BSt500$_s$ specimen

Material yield stress, MPa	Tensile strength, MPa	Elastic modulus, GPa	Elongation, % (after breaking)
Ribbed bar ≥500	≥550	200	≥12

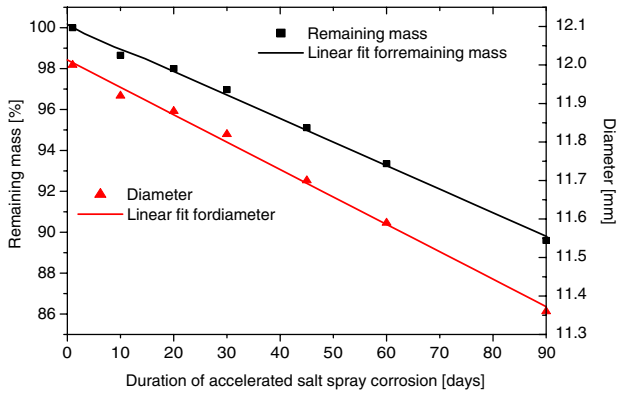

Fig. 1 Correlation of remaining mass and diameter reduction vs. corrosion duration for 12 mm diameter BSt500$_s$ specimens

2.3 High-Cycle Fatigue

The effect of corrosion on the fatigue and life expectancy of BSt500$_s$ 12 mm diameter steel bars was investigated through a series of 60 laboratory experiments. After the salt spray corrosion process the uniaxial fatigue of the specimens was measured according to ISO/FDIS 15630-1 method. These tests were carried out at fatigue levels of ±325, ±265, and ±200 MPa, stress ratio $R = -1$, frequency of 20 Hz and the conventional fatigue limit was determined for life expectancy of $N_f = 8.1 \times 10^6$ cycles. These tests were performed in non-corroded and corroded specimens that had been exposed to salt spray for 15 and 30 days respectively and which resulted in three Woehler curves, utilizing 12 out of each group of 20 tests for their construction, while the remaining eight were spares. The minimum specimen length had to be 14xd, but the ones used were 280 mm long of which 55 mm length was used under each grip and 170 mm was the free length in order to facilitate loading in the testing machine.

The experimental results are displayed in Fig. 4 through Woehler S-N diagrams for noncorroded and corroded for 15 and 30 days specimens accordingly and the progressive reduction in fatigue strength can be realized as a function of the corrosion level. These curves are described with the following Weibull function:

$$d = C_1 + \frac{C_2 - C_1}{e^{(\log t/C_3)^{C_4}}} \qquad \text{(Eq 2)}$$

whose constants are shown in Table 2.

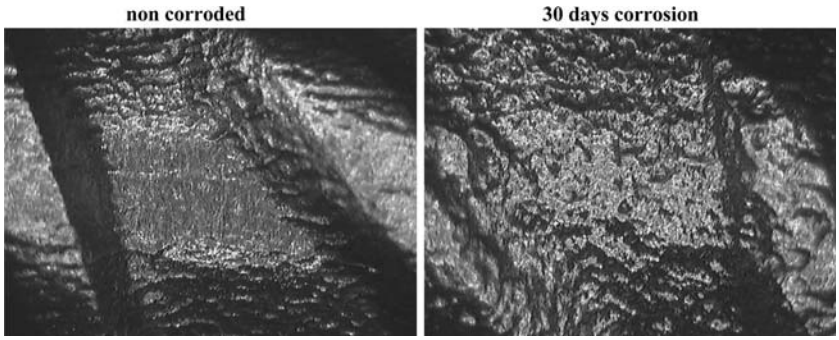

Fig. 2 Stereoscopic images of specimens

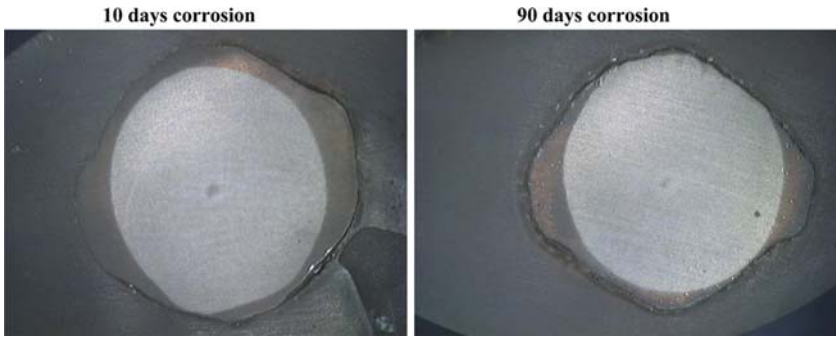

Fig. 3 Decrease of the martensitic layer as a result of corrosion duration

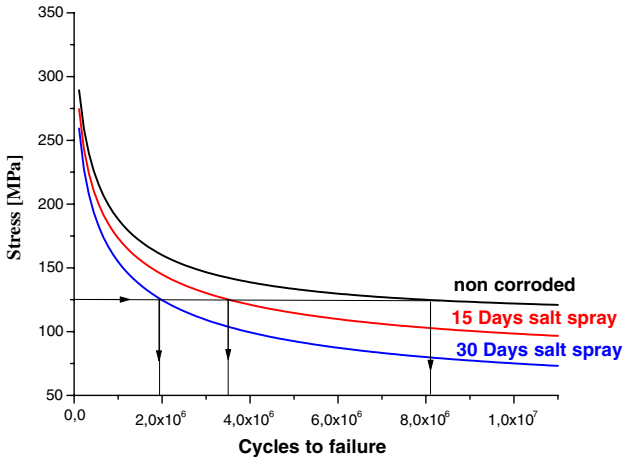

Fig. 4 Woehler S-N fatigue diagrams for noncorroded and corroded specimens

Table 2 Weibull constants

	Noncorroded	15 days salt spray	30 days salt spray
C1	113.50884	75.97808	50.65955
C2	379.73621	401.14345	383.98002
C3	5.78098	5.78626	5.82995
C4	6.46082	5.16244	5.25499

2.4 Low-Cycle Fatigue

The effect of corrosion on low-cycle fatigue behavior of $BSt500_s$ tempcore steel under earthquake conditions was investigated, subjected to uniaxial sinusoidal loads of 1 Hz frequency and constant strain amplitude of ±1% and 2.5% after being exposed to salt spray for different times. A total of 42 low-cycle fatigue tests were conducted, 3 for each corrosion level at 0, 10, 20, 30, 45, 60, and 90 days and for ±1 and 2.5% strain levels. The 12 mm diameter specimens were cut at 172 mm length and the free length between grips was set at an empirical value of $6 \times 12 = 72$ mm, since it represents typically the free bar length between stirrups in critical regions of columns in seismic areas.

Modification in the geometry, in order to comply with the ASTM E606 standards for strain controlled fatigue testing, would alter the nature of the material thus giving misleading results. Therefore, the specimens were subjected to low-cycle fatigue testing without modifications of their cross-sectional area. The analytical expression for total strain is given by (Ref 33):

$$\frac{\Delta\varepsilon_t}{2} = \frac{\Delta\varepsilon_e}{2} + \frac{\Delta\varepsilon_p}{2} = \frac{\sigma'_f}{E}(2N)^b + \varepsilon'_f(2N)^c \qquad \text{(Eq 3)}$$

where $\Delta\varepsilon_t$, $\Delta\varepsilon_e$ and $\Delta\varepsilon_p$ are the total, elastic and plastic strain amplitudes respectively, as shown in the steady state loops of Fig. 5 and 6, ε'_f and c are the fatigue ductility coefficient and exponent respectively, σ'_f and b are the fatigue strength coefficient and exponent respectively and E is the modulus of elasticity. Three typical low-cycle fatigue stress-strain (hysterisis loops) diagrams of 10-15, 250-255 and 500-505 cycles respectively of noncorroded are shown in Fig. 5 where progressive reduction of stress is observed. From the low-cycle fatigue tests, the total dissipated energy density was evaluated

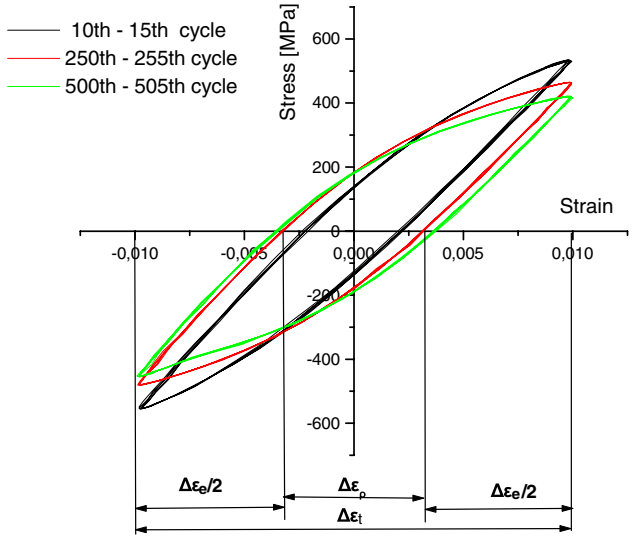

Fig. 5 Typical low-cycle fatigue stress-strain diagrams, at ±1% applied strain, showing hysterisis loops for initial, middle and final cycles for noncorroded steel

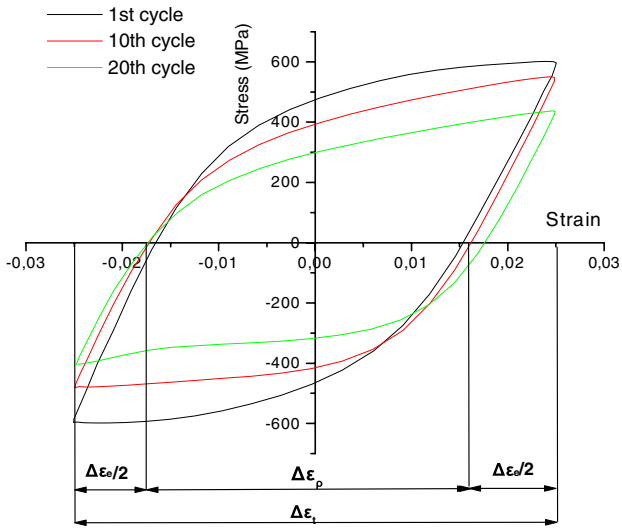

Fig. 6 Typical low-cycle fatigue stress-strain diagrams, at ±2.5% applied strain, showing hysterisis loops for the 1st, 10th, and 20th cycles for noncorroded steel

as the sum of the areas formed within the hysterisis loops. This is a measure of the capacity of the material to absorb energy during seismic activity. After evaluating the total energy absorbed the remaining energy density was plotted after each cycle as a function of the number of subjected cycles.

Figure 6 shows three typical low-cycle fatigue stress-strain diagrams (hysterisis loops) the 1st, 10th, and 20th cycles for noncorroded steel at ±2.5% applied strain where progressive reduction of stress is observed.

Even though Fig. 5 and 6 represent random noncorroded specimens it is clearly shown that plastic deformation ($\Delta\varepsilon_p$) appears to be an increased impact factor. Therefore since the plastic deformation ($\Delta\varepsilon_p$) of Fig. 5 occupies the 33.5% of the applied width at ±1% strain level as expected, this amount is increased to 66.5% when the strain level is ±2.5% as indicated

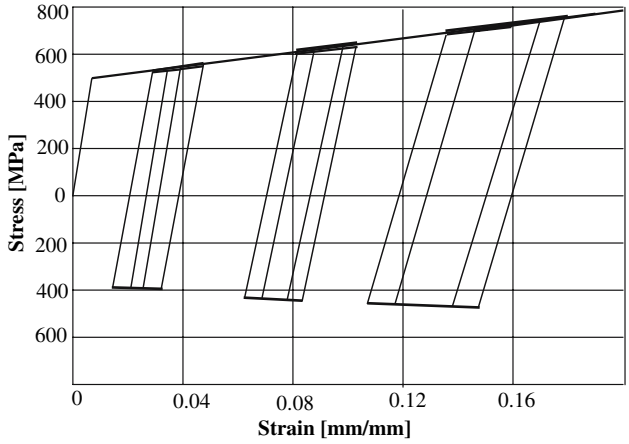

Fig. 7 Steel stress-strain history as predicted on the basis of plasticity theory

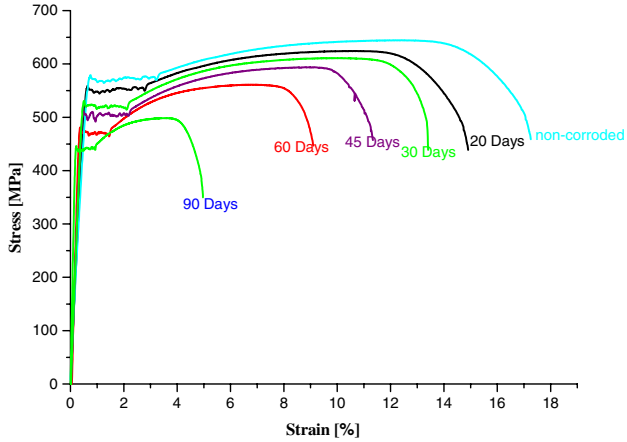

Fig. 8 Reduction of elongation and energy density of different corrosion levels

in Fig. 6. The measured plastic deformation corresponds approximately to the average life expectancy of the material.

Figure 7 shows data for steel reinforcement subjected to reversed cyclic loading. Group cycling indicate the strain history observed in actual structures (Ref 34). Therefore it is evident that cycling with large or small strain amplitudes are additive and highly reduce the useful life expectancy of steel in accordance to plasticity theory. Knowing the mechanical behavior of the gradually corroded steel (Ref 17, 35) and as shown in Fig. 8, the reduction in ductility properties such as elongation and energy density, is evident. It is finally apparent that the reduction of the useful life of steel is closely related to the loading history, the width of the subjected strain and the imposed corrosion level.

Figure 9 shows that inspection of steel reinforcement after 65% of the useful service life of noncorroded steel indicates that it is possible that a number of steel bars with initial gage diameter of 12 mm, corrosion level greater than 4.89% and remaining diameter of 11.70 mm will have already failed. For a more conservative inspection at 50% of the useful service life of the noncorroded steel, there is a possibility of partial reinforcement failure with corrosion level exceeding 6.65% and remaining diameter 11.59 mm. In addition the correlation of the remaining energy density vs. the imposed number of cycles after which the specified threshold is not met, as a proportion of the total number of cycles to failure of the noncorroded specimens is indicated.

Since the low-cycle fatigue tests were performed at constant strain amplitude, the maximum resisting force exerted by the specimens for each cycle was gradually reduced. Figure 5, 6, 10, and 11 shows that a rapid drop of the applied force occurred during the first few cycles, followed by gradual reduction of this force for most of the specimens' life and a new rapid drop, which continued until failure. Furthermore, an overall reduction of the applied force was observed for the pre and postcorroded specimens. This was expected since the cross-sectional area was reduced with advancing corrosion. The reinforcing steel used in structures is expected to carry a constant load throughout its service life since these loads remain fairly constant over time. Figure 10 and 11 shows that for a threshold of 80% of the maximum force of the noncorroded material and as corrosion progresses, the remaining life for which the material can sustain this force is greatly reduced.

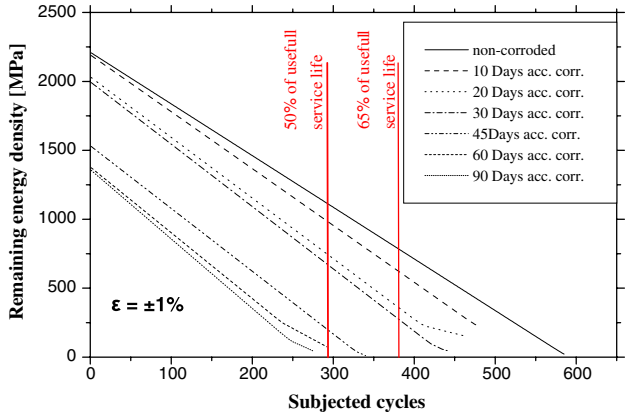

Fig. 9 Correlation of remaining energy density and subjected cycles for ε = ±1%

Table 3 shows the steel specimens' failure behavior vs. salt spray exposure duration, total dissipated energy density and cycles to failure before and after the 80% threshold load limit. As corrosion levels increase, the number of cycles to failure decreases. Since the total dissipated energy is the sum of the hysterisis loops formed, it would be expected that the percent reduction of the number of cycles to failure would be the same as that of the total dissipated energy.

3. Results

Corrosion was found to be very important for the integrity of steel and pitting became evident after a few days of salt spray. It became progressively more severe as the corrosion level increased. As the steel surface became rougher, cavities, and notches were formed, which reduced locally the steel surface diameter below the average value. Considerable reduction in the fatigue limit took place since the mass loss led to reduction of the exterior hard layer of martensite and a drastic drop in the energy density of the corroded specimens. This developed stress concentration points, which were highly localized at imperfections and especially in the pits and notches of the rib bases of the

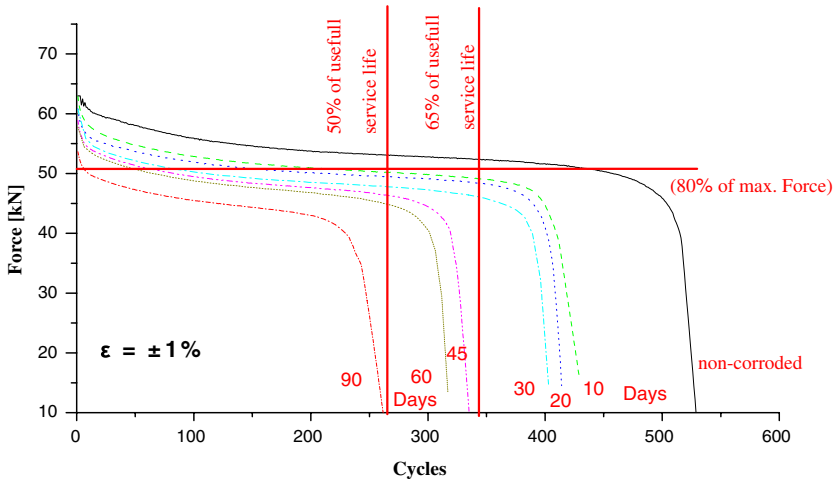

Fig. 10 Typical life expectancy of steel before the load capacity drops below 80% of the maximum value for ±1% strain level

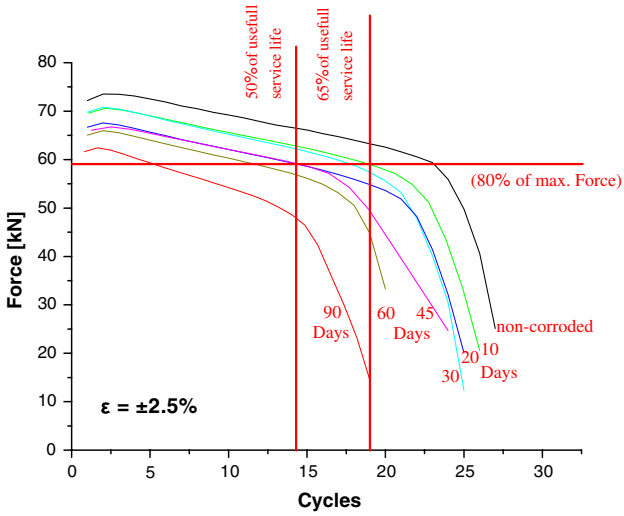

Fig. 11 Typical life expectancy of steel before the load capacity drops below 80% of the maximum value for ±2.5% strain level

corroded steel. Thus, the increased corrosion led to a decrease of the useful life of steel. From Fig. 1 it can be seen that the mass loss, or wear rate, for corroded vs. noncorroded 12 mm nominal diameter steel specimens, for 15 and 30 days corrosion level, was of the order of 1.50-3.03%, accordingly. Table 4 shows the mass loss and remaining mass vs. corrosion level. It was observed that a small mass loss created great reduction in the strength and life expectancy of steel. The rib height was also measured during the different levels of corrosion and at 90 days, corresponding to 10.40% mass loss, the average height of the ribs was reduced by approximately 80-85%.

From Fig. 4 it can be seen that for steel corroded for 15 and 30 days, corresponding to 1.50 and 3.03% mass loss, and for a hypothetical applied stress of 125 MPa and stress ratio $R = -1$, the life expectancy is reduced from 8.1×10^6 cycles of the noncorroded case, to 3.50×10^6 and 1.95×10^6 cycles, respectively. In other words the life expectancy of steel is reduced approximately by 55-75%. This is very significant for aggressive climatic conditions such as the ones existing in the coastal areas of Greece where salinity high heat, humidity, and earthquakes are predominant factors.

The stress-strain behavior shown in Fig. 5 and 6 indicate data for reinforcing steel subjected to a reversed cyclic strain with symmetric inelastic strain intervals. In engineering practice such data exhibit particular response characteristics that are not obviously realized by tensile tests data. Important characteristics of response shown in Fig. 5, 6, 8, and Table 3 include:

(a) The specimens exhibit loss in linearity during unloading, known as Bauschinger effect, prior to achieving the yield strength in the opposite direction.
(b) The specimens exhibit isotropic strain hardening characterized by increasing strength under increasing inelastic strain demand. This is observed under cyclic as well as monotonic loading.
(c) The initial tangent to the unloading stress-strain response is slightly less than the initial elastic stiffness.
(d) The specimens exhibit cyclic strain softening, known also as reduced tangential stiffness, under multiple cycles to particular strain limits.

Figure 8 shows the stress-strain behavior vs. corrosion level and the energy density as the area under these curves. Energy density indicates the ability that a steel bar has to absorb energy from external loads without danger of failure. It can be observed that as the corrosion level increases the strength properties (yield and fracture points) and the ductility properties (energy density and elongation to fracture) decrease (Ref 17, 35). In harsh environments and seismic areas steel bars must have great amounts of energy density (Ref 36). Considerable reduction in energy density is observed as the duration of corrosion is increased. In addition the noncorroded material has greater energy density than any of the corroded bars. The experimental results of uniaxial fatigue tests have shown an overall degradation of the corroded $BSt500_s$ steel reinforcing bars. The formation of an oxide layer on the surface of the specimens made them rougher by forming pits, notches, and cavities. This allowed for formation of stress concentration points leading to cumulative damage under alternating fatigue loading. Furthermore, the oxide layer reduced the nominal cross-sectional area of the specimens. Considerable degradation of the steel specimens due to corrosion creates a drop in energy

Table 3 Low-cycle fatigue failure behavior of pre and post corroded steel

	Total dissipated energy density, MPa		Cycles to failure		Cycles before load capacity drops below 80% of the maximum value	
	Strain level		Strain level		Strain level	
Duration of salt spray corrosion	±1%	±2.5%	±1%	±2.5%	±1%	±2.5%
Noncorroded	2329	753	529	28	457	23
10 days	2262	689	429	27	280	22
20 days	2168	667	414	27	207	20
30 days	2117	659	403	27	108	16
45 days	1643	647	335	26	81	13
60 days	1430	615	317	25	64	13
90 days	1403	528	263	23	10	8

Table 4 Mass loss and remaining diameter at different corrosion levels

Exposure to salt spray corrosion environment							
Exposure time, days	0	10	20	30	45	60	90
Mass loss, %	0	1.35	2.00	3.03	4.89	6.65	10.40
Diameter, mm	12.00	11.92	11.88	11.82	11.70	11.59	11.36

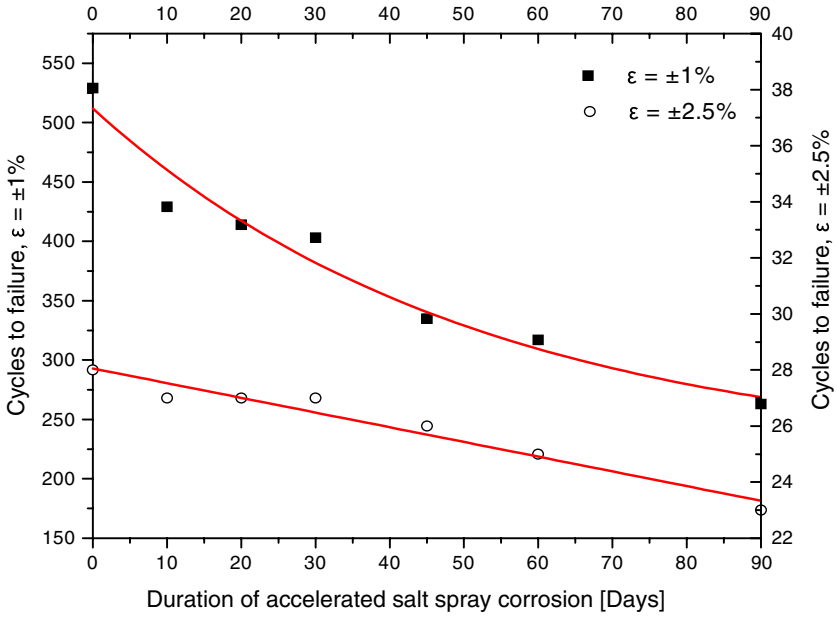

Fig. 12 Correlation of the cycles to failure at ±1% and ±2.5% strain vs. corrosion level

density, Fig. 8, combined with the gradual loss of the exterior hard layer of martensite, Fig. 3.

Figure 10 and 11 indicates that for a threshold of 80% of the maximum force of the noncorroded material and as the corrosion level increases, the remaining life for which the material can support this force is greatly reduced. In addition, if the number of cycles to failure is considered unaffected by corrosion, as is the case of code regulation which account for the use of steel reinforcement in concrete, then failure may occur much sooner than expected (Ref 34, 37).

Figure 12 shows the correlation of the cycles to failure at 1 and 2.5% strain vs. corrosion level. It can be seen that as the corrosion level increases at ±1% strain, the life of the material decreases drastically, while for ±2.5% strain level the life of the material which has been reduced already by approximately 54% decreases at a slower rate.

4. Conclusions

The effect of corrosion on mass loss and on high- and low-cycle fatigue of $BSt500_s$ steel has shown that:

1. The mass loss for corroded vs. noncorroded steel for 10-90 days corrosion level was of the order of 1.35-10.40%,

accordingly. A small mass loss created great reduction in the strength and life expectancy of steel for low-cycle fatigue loading.

2. Corrosion was initiated at the base of the ribs and as it progressed the rib size was reduced and at 90 days, corresponding to 10.40% mass loss, their average size was reduced by approximately 80%. This has also a direct impact on the bonding mechanism of reinforced concrete structures.
3. Considerable reduction in the fatigue limit took place due to partial loss of the exterior hard layer of martensite and drastic drop in the energy density of the corroded specimens thus developing stress concentration points which are highly localized at the imperfections and especially in the pits and notches of the rib bases. Thus the increased corrosion shortened the useful life of steel.
4. In actual engineering practice the strain history and the energy density are overlooked by the codes and should be re-evaluated, accordingly.
5. The maximum load-bearing capacity was reduced during low-cycle fatigue loading and further reduction is observed for corroded specimens. Older structures in earthquake prone areas are not expected to display a constant load bearing ability beyond a certain service life. Progression of corrosion caused significant reduction of ductility and life expectancy.

References

1. C. Fang, K. Lundgren, L. Chen, and C. Zhu, Corrosion Influence on Bond In Reinforced Concrete, *Cement Concr. Res.*, 2004, **34**, p 2159–2167
2. G.J. Al-Sulaimani, M. Kaleemullah, and I.A. Basunbul, Rasheeduzzafar, Influence of Corrosion and Cracking on Bond Behaviour and Strength of Reinforced Concrete Members, *Proc. A.C.I. 2* , 1990, p 220–231
3. X. Fu and D.D.L. Chung, Effect of Corrosion on the Bond between Concrete and Steel Rebar, *Cement Concr. Res.*, 1997, **27**(12), p 1811–1815
4. R. Capozucca, Damage to Reinforced Concrete Due to Reinforcement Corrosion, *Constr. Build. Mater.*, 1995, **9**(5), p 295–303
5. Z.P. Bazant, Physical Model for Steel Corrosion in Concrete Sea Structures-Theory, *J. Struct. Div.*, 1979, **105**, p 1137–1153
6. A.A. Almusallam, A.S. Al-Gahtani, and A.R. Aziz, Rasheeduzzafar, Effect of Reinforcement Corrosion on Bond Strength, *Constr. Build. Mat. J.*, 1996, **10**(2), p 123–129
7. A.A. Almusallam, A.S. Al-Gahtani, A.R. Aziz, and F.H. Dakhil, Rasheeduzzafar, Effects of Reinforcement Corrosion on Flexural Behavior of Concrete Slabs, *J. Mat. Civil Eng.*, 1996, **8**(3), p 123–127
8. G.M. Sheng and S.H. Gong, Investigation of Low Cycle Fatigue Behaviour of Building Structural Steels Under Earthquake Loading, *Acta Metall. Sin. (English Letters)*, 1997, **10**(1), p 51–55
9. T. Yoshaki, *Proceedings of Academical Lectures of JAS* (Tokyo), 1983, p 606
10. H. Shigeru, Research Report, "Retrofitting of Reinforced Concrete Moment Resisting Frames," Supervised by Park, R and Tanaka, H. ISSN0110-3326, August 1995
11. G.K. Glass and N.R. Buenfeld, Chloride-Induced Corrosion of Steel in Concrete, *Prog. Struct. Eng. Mater.*, 2000, **2**(4), p 448–458
12. M. Maslehuddin, I.M. Ibrahim, S. Huseyin, and A.L. Al-Mana, Influence of Atmospheric Corrosion on the Mechanical Properties of Reinforcing Steel, *Constr Build Mater*, 1993, **8**(1), p 35–41
13. C. Fang, K. Lundgren, L. Chen, and C. Zhu, Corrosion Influence on Bond in Reinforced Concrete. *Cement Concr. Res.*, 2004, **34**(11), p 2159–2167
14. J.P. Broomfield, *Corrosion of Steel in Concrete*. E & FN Spon, London, 1997, 22
15. V.G. Papadakis , *Supplementary Cementing Materials in Concrete Activity, Durability and Planning*, Danish Technological Institute Concrete Center, 1999
16. M.G. Alvarez and J.R. Galvele, The Mechanisms of Pitting of High Purity Iron in NaCl Solutions, *Corros. Sci.*, 1984, **24**, p 27–48
17. C.A. Apostolopoulos, M.P. Papadopoulos, and Sp.G. Pantelakis, Tensile Behavior of Corroded Reinforcing Steel Bars BSt 500_s, *Construct. Build. Mater.*, 2006, **20**(9), p 782–789
18. J. Cairns, G.A. Plizzari, Y. Du, D.W. Law, and C. Franzoni, Mechanical Properties of Corrosion-Damaged Reinforcement, *ACI Mater. J. Technical Paper*, 102-M29, 2005, **102**(4), p 256–264
19. G.C. Koch, M.P. Brongers, M.P. Thompson, Y.P. Virmani, and J.H. Payer, "Corrosion Costs and Preventive Strategies in The United States," Federal Highway Administration, Washington, D.C, Report No. FHWA-RD, 2002, p 01–156
20. G. G. Clementa, "Testing of Selected Metallic Reinforcing Bars for Extending the Service Life of Future Concrete Bridges," Final report, Virginia Transportation Research Council, Charlottesville, VA, VTRC 03-R7, 2002
21. X. Wang and X. Liu, Bond Strength Modelling for Corroded Reinforcements, *Constr. Build. Mater.*, 2006, **20**(3), p 177–186
22. J.G. Cabrera, Deterioration of Concrete Due to Reinforcement Steel Corrosion, *Cement Concr. Compos.*, 1996, **18**(l), p 47–59
23. P. Riva, A. Franchi, and D. Tabeni, Weld Tempcore Reinforcement Behavior for Seismic Applications, Materials and Structures, *Mater. Struct.*, 2001, **34**, p 240–247
24. A. Franchi, P. Riva, P. Ronca, R. Roberti, and M. La Vecchia, Failure Modalities of Reinforcement Bars in Reinforced Concrete Elements Under Cyclic Loadind, *Studi e rocerche*, 1996, **17**, p 157–187
25. M. Pipa and A. Vercesi, "Cyclic Tests of Grade B400 and B500 Tempcore Bars," PREC8 Report, LNEC, 1996
26. M. Pipa, E.C. Carvalho, and A. Otes, Experimental Behaviour of R.C. Beams with Grade 500 Steel, *Proceedings of 10th European Conference on Earthquake Engineering* (Vienna) 1994.
27. P. Schiessl, "Corrosion of Steel in Concrete," RILEM Report TC 60-CSC, 1988
28. K. Stanish, R.D. Hooton, and S.J. Pantazopoulou, Corrosion Effects on Bond Strength in Reinforced Concrete, *ACI Struct. J.*, 1999, **96**(6), p 915–921
29. H.S. Lee, T. Noguchi, and F. Tomosawa, Evaluation of the Bond Properties between Concrete and Reinforcement as a Function of the Degree of Reinforcement Corrosion, *Cement Concr. Res.*, 2002, **32**(8), p 1313–1318
30. J.G. Cabrera and P. Ghoddoussi, Effect of Reinforcement Corrosion on the Strength of the Steel Concrete Bond, *Int. Conf., Bond in Concrete—from Res. to Pract.*, vol. 3 (Riga, Latvia), 1992, p 10.11–10.24
31. S.Y.M. Ma, V.V. Bertero, and E.P. Popov, Experimental and Analytical Studies on the Hysteretic Behavior of Reinforced Concrete Rectangular and T-Beams, *Earthquake Engineering Research Report*, vol. 76(2) (Berkeley), University of California, 1976
32. G. Chang and J. Mander, "Seismic Energy Based Fatigue Damage Analysis of Bridge Columns: Part I-Evaluation of Seismic Capacity", NCEER Technical Report 94-0006, 1994
33. H.O. Fuchs and R.I. Stephens, *Metal Fatigue in Engineering*. John Wiley & Sons Inc, USA, 1980, 76–82
34. Hellenic Anti-Seismic code 2000 (EAK2000) no. Δ17a/20.12.2000 (Government Gazette ISSUE) 2184B, (2001) Athens
35. Y.G. Du, L.A. Clark, and A.H.C. Chan, Effect of Corrosion on Ductility Of Reinforcing Bars, *Magazine Concr. Res.*, 2005, **57**(7), p 407–419
36. G.C. Sih and C.K. Chao, Failure Initiation in Unnotched Specimens Subjected to Monotonic and Loading, *Theor. Appl. Fract. Mech.*, 1984, **2**, p 67–73
37. CEN Technical Committee 250/SC8, "EUROCODE 8: Earthquake Resistant Design of Structures-Part 1: General Rules and Rules for Buildings (ENV 1998-1-1/2/3)," CEN, Berlin, 1995